

# Nonflammable, Low-Cost, and Fluorine-Free Solvent for Liquid Electrolyte of Rechargeable Lithium Metal Batteries

Tianwei Jin,<sup>†,ID</sup> Yini Wang,<sup>†</sup> Zeyu Hui,<sup>†</sup> Boyu Qie,<sup>†</sup> Aijun Li,<sup>†,§</sup> Daniel Paley,<sup>‡</sup> Bingqing Xu,<sup>†,⊥</sup> Xue Wang,<sup>†,¶ID</sup> Adrian Chitu,<sup>†</sup> Haowei Zhai,<sup>†,ID</sup> Tianyao Gong,<sup>†</sup> and Yuan Yang<sup>\*†,ID</sup>

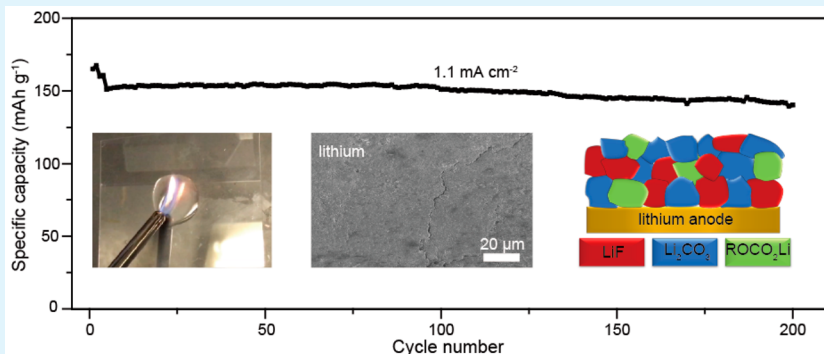
<sup>†</sup>Program of Materials Science and Engineering, Department of Applied Physics and Applied Mathematics and <sup>‡</sup>Columbia Nano Initiative, Columbia University, New York, New York 10027, United States

<sup>§</sup>Key Laboratory of Orogenic Belts and Crustal Evolution, School of Earth and Space Sciences, Peking University, Beijing 100871, P.R. China

<sup>⊥</sup>State Key Laboratory of New Ceramics and Fine Processing, School of Materials Science and Engineering, Tsinghua University, Beijing 100084, P.R. China

<sup>¶</sup>Center for Composite Material and Structure, School of Astronautics, Harbin Institute of Technology, Harbin 150001, P.R. China

## S Supporting Information



**ABSTRACT:** Rechargeable metallic lithium batteries are considered as promising candidates for next-generation energy storage due to their high energy densities. However, safety concerns associated with electrolyte flammability and dendrite growth hinder their practical applications. Nonflammable liquid electrolytes have attracted significant attention recently, but they are mainly based on expensive ionic liquids, fluorinated solvents, or with highly concentrated salt. Here we design a novel trisalt electrolyte composed of lithium bis(trifluoromethanesulfonyl)imide (LiTFSI)-lithium bis(oxalato)borate (LiBOB)-LiPF<sub>6</sub> in EC/PC solvent, which is not flammable even in contact with fire. Moreover, it creates unique protection of solid electrolyte interphase (SEI) film on lithium metal anode that allows 400 cycles of Li/Li(NiMnCo)<sub>1/3</sub>O<sub>2</sub> cells with a capacity retention of 97.0% at 0.83 mA cm<sup>-2</sup>. This work illustrates that low-cost fluorine-free carbonate solvents can also realize nonflammable electrolyte with high performance, which opens new opportunities to promote safety and energy density of rechargeable lithium batteries simultaneously.

**KEYWORDS:** lithium metal battery, nonflammability, fluorine-free, low freezing point, rate-capability

## 1. INTRODUCTION

Lithium-based rechargeable batteries have been used widely in portable electronics, electric vehicles, and grid-level energy storage.<sup>1–4</sup> One major challenge for lithium batteries is its high flammability, as conventional carbonate electrolytes have low flash points around room temperature, and thus, lithium batteries can easily catch fire by heat generated in thermal runaway.<sup>5,6</sup> Such thermal instability is becoming even more severe along with the pursuit of higher energy density, which utilizes more unstable materials with high charge capacity such as the lithium metal anode and high nickel oxides cathodes.<sup>7,8</sup>

State-of-the-art battery electrolytes mainly consist of ethylene carbonate (EC), acyclic carbonate (e.g., dimethyl

carbonate/DMC, diethyl carbonate/DEC), and LiPF<sub>6</sub> as the salt. Their low flash points originate from acyclic carbonates (e.g., 17 °C for DMC and 33 °C for DEC), while EC has a high flash point of 160 °C.<sup>9,10</sup> Moreover, LiPF<sub>6</sub> has a low decomposition temperature below 100 °C,<sup>11</sup> which accelerates heat generation in the battery electrolyte. Various approaches have been explored to improve thermal stability of organic carbonate electrolytes such as the addition of ionic liquid,<sup>12,13</sup> flame-retardant additives,<sup>14,15</sup> and concentrated electro-

Received: December 19, 2018

Accepted: April 23, 2019

Published: April 23, 2019

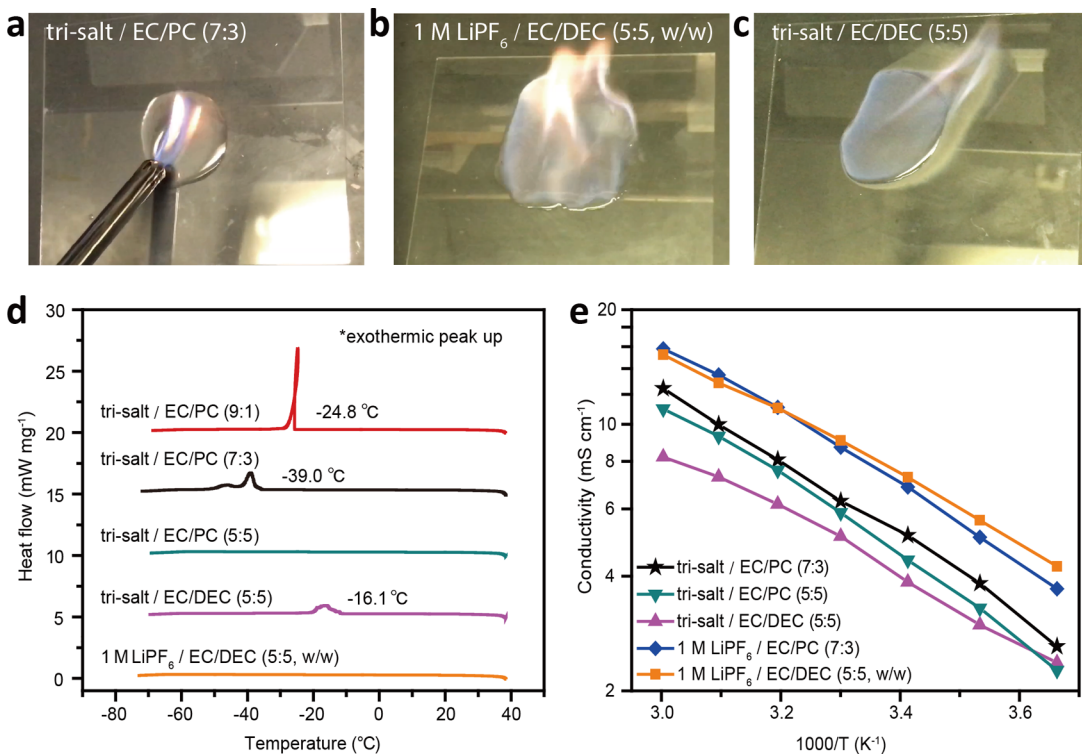


**Figure 1.** Flammability, thermal properties, and ionic conductivities of different electrolytes. (a–c) Flammability test of 0.5 mL (a) trisalt in EC/PC (7:3), (b) 1 M LiPF<sub>6</sub> in EC/DEC (5:5, w/w), and (c) trisalt in EC/DEC (5:5); (d) DSC heat-flow profiles of five kinds of electrolytes from 40 °C to -70 °C. The exothermic peaks are labeled. (e) Temperature dependence of ionic conductivities of different electrolytes. All ratios mentioned are volume ratios, except for 1 M LiPF<sub>6</sub> in EC/DEC.

lytes.<sup>16,17</sup> However, the use of ionic liquids, high portion of salt, and the addition of fluorinated solvents lead to significant higher cost.<sup>18,19</sup>

One alternative approach is to reduce the use of acyclic carbonate and LiPF<sub>6</sub> in commercial electrolyte to increase electrolyte's thermal stability. However, other key properties should not be significantly compromised in developing such new electrolyte, especially ionic conductivity, temperature window, and electrochemical window. Propylene carbonate (PC) is an attractive candidate due to its low melting point (-49 °C), high flash point, and high dielectric constant.<sup>10</sup> Unfortunately, PC is considered to have a poor cycling efficiency toward lithium metal anode.<sup>20</sup> Nonuniform Li deposition caused by the inhomogeneous SEI components from PC decomposition will break the SEI layer and lead to further irreversible Li loss.<sup>21</sup> To address this issue, here we adopt two approaches. The first one is to reduce the portion of PC in the EC/PC electrolyte. Thanks to the low melting point of PC, 70%/30% EC/PC mixture (v/v) has the same liquidus temperature as 50%/50% EC/DEC mixture (v/v) and 65%/35% EC/DMC mixture (v/v).<sup>22</sup> Therefore, the reduction of PC concentration will not remarkably compromise the temperature window of as-prepared electrolyte. Second, a trisalt system of LiTFSI-LiBOB-LiPF<sub>6</sub> has been reported to form a robust SEI layer on anode, stabilize the aluminum current collector, and better protect NMC cathode in EC/EMC solvent,<sup>23,24</sup> which probably can be employed to restrain the problems of PC through forming a durable and relatively uniform SEI. Moreover, such trisalt system only contains 5 at% LiPF<sub>6</sub>, while the other two salts, LiTFSI/LiBOB are thermally stable up to 300 °C,<sup>25,26</sup> which further reduces heat generation due to salt decomposition.

By combining two strategies above, here we report a new fire-retardant trisalt electrolyte system, LiTFSI-LiBOB-LiPF<sub>6</sub> in EC/PC, which is not ignitable by fire. We further apply it to Li/LiNi<sub>1/3</sub>Mn<sub>1/3</sub>Co<sub>1/3</sub>O<sub>2</sub> (NMC) rechargeable batteries, delivering over 200 cycles with a high Coulombic efficiency (CE) of 99.7% at a current density of 1.1 mA cm<sup>-2</sup> and charge capacity of 1.1 mAh cm<sup>-2</sup>. Long cycle life of 400 cycles with a capacity retention of 97.0% is also achieved with an additional piece of poly(vinylidene fluoride-*co*-hexafluoropropylene) (PVdF-HFP) separator. The nonflammable solvent system endows the electrolyte with great safety even when exposed to fire directly. Moreover, the trisalt system helps form a robust SEI film on lithium to allow a significantly improved cycling stability, revealing the possibility of the EC/PC solvent combination to realize reliable electrolytes with high thermal stability.

## 2. RESULT AND DISCUSSION

The thermal stability of the reported trisalt (0.6 M LiTFSI/0.4 M LiBOB/0.05 M LiPF<sub>6</sub>) in EC/PC electrolyte and control samples was first tested by exposing 0.5 mL of electrolyte to a butane candle lighter fire. Three different volume ratios of EC:PC were tested including 9:1, 7:3, and 5:5. All of the trisalt/EC/PC electrolytes are not ignitable (Figure 1a and Video S1), possibly due to the high flash points of EC and PC. By contrast, trisalt in EC/DEC (5:5, v/v) and 1 M LiPF<sub>6</sub> in EC/DEC (5:5, w/w), which is one of the conventional electrolytes, catch fire immediately when exposed to flame (Figure 1b,c and Video S2). To further clarify whether the nonflammability originates from solvent or salt, single-salt (1 M LiPF<sub>6</sub>) and dual-salt (0.6 M LiTFSI/0.4 M LiBOB) in EC/PC (7:3, v/v) were also tested by the same method, as shown

**Table 1.** Thermal and Electrochemical Information of Trisalt in Different EC/PC Solvents

electrolyte	flammability	freezing point (°C)	conductivity at 20 °C (mS cm <sup>-1</sup> )	capacity fading per 100 cycles <sup>a</sup>
trisalt in EC/PC (5:5, v/v)	nonflammable	N/A <sup>b</sup>	4.4	12.5%
trisalt in EC/PC (7:3, v/v)	nonflammable	-15.0	5.1	3.7%
trisalt in EC/PC (9:1, v/v)	nonflammable	-1.0	not measured	not measured
1 M LiPF <sub>6</sub> in EC/PC (7:3, v/v)	nonflammable	< -20	6.9	52.4%
1 M LiPF <sub>6</sub> in EC/DEC (5:5, w/w)	flammable	< -20	7.2	15.8%

<sup>a</sup>In Li/NMC batteries with current density of 1.1 mA cm<sup>-2</sup> after two cycles at 0.11 mA cm<sup>-2</sup> and two more cycles at 0.37 mA cm<sup>-2</sup>. <sup>b</sup>This value is not measured due to its difficult crystallization process.<sup>29</sup>

in **Video S3**. Both of them are not ignitable, indicating that the use of EC/PC significantly improves the thermal stability of electrolytes compared to commercial electrolytes with acyclic carbonates, which helps enhance the safety of rechargeable lithium batteries. These results are summarized in **Table 1**.

One common concern for nonflammable electrolytes is that their liquid windows are typically limited and thus the low temperature performance is poor, restraining them from practical applications. To investigate this potential issue, differential scanning calorimeter (DSC) was used to measure thermal behavior of different electrolytes, as shown in **Figure 1d**. The DSC curves of trisalt in EC/PC (5:5, v/v) and 1 M LiPF<sub>6</sub> in EC/DEC (5:5, w/w) show no exothermic peak down to -70 °C, while trisalt in EC/PC (7:3, v/v), EC/PC (9:1, v/v), EC/DEC (5:5, v/v) show exothermic peaks at -39.0 °C, -24.8 °C, and -16.1 °C, respectively. The exothermic peak-free behavior is likely a result of supercooling and the electrolytes' relatively low freezing points.<sup>27,28</sup> To mimic real scenario, the freezing points of trisalt in EC/PC (7:3, v/v) and EC/DEC (5:5, v/v) were measured again via cooling in a solution bath, which are -15.0 °C and -14.5 °C, respectively (**Figure S1b,c**), indicating acceptable and comparable temperature windows at the low ends in these two solvent systems (details described in the **Experimental Section**). High EC/PC ratio (9:1, v/v) with trisalt has a higher freezing point of -1.0 °C (**Figure S1d**), which is not satisfying for practical applications. In addition, 1 M LiPF<sub>6</sub> in both EC/PC (7:3, v/v) and EC/DEC (5:5, w/w) show low freezing points below -20 °C (**Figure S1e**), indicating that the freezing point of an electrolyte is significantly influenced by salt in addition to solvent. On the basis of these data, EC/PC solvent system exhibits a great potential to improve low temperature performance by adjusting salts inside.

To further investigate the low temperature behavior of EC/PC-based electrolytes, temperature dependence of electrolyte conductivities was measured from 0 to 60 °C (**Figure 1e**). The 1 M LiPF<sub>6</sub> in EC/PC (7:3, v/v) displays comparable conductivity with 1 M LiPF<sub>6</sub> in EC/DEC (5:5, w/w), such as 6.9 versus 7.3 mS cm<sup>-1</sup> at 20 °C, and 3.7 versus 4.2 mS cm<sup>-1</sup> at 0 °C. Meanwhile, although the trisalt in EC/PC (7:3, v/v) electrolyte has lower conductivity, it still reaches 5.1 and 2.6 mS cm<sup>-1</sup> at 20 and 0 °C, respectively. The value at 20 °C is at the highest level among previous notable reports on nonflammable electrolytes (1.0–5.1 mS cm<sup>-1</sup>).<sup>13,14,16–19</sup> The trisalt in EC/PC (5:5, v/v) electrolyte also shows similar conductivity. In summary, EC/PC (7:3, v/v) and EC/PC (5:5, v/v) solvents combination exhibit favorable nonflammability and low temperature behaviors, signifying their possible application into the electrolyte systems for lithium batteries.

To investigate the best ratio of EC:PC and the electrochemical performance of trisalt in EC/PC electrolytes,

electrolytes discussed above were combined with metallic lithium anodes and NMC cathodes for galvanostatic cycling. Prior to the cycling at 1 C (1.1 mA cm<sup>-2</sup>), two cycles at C/10 followed by two more cycles at C/3 were carried out to form SEI with good quality. **Figure 2a** shows their cycling performance in Li/NMC batteries. For trisalt in EC/PC (7:3, v/v) electrolyte system, the initial discharging capacity at 1C rate is 151.0 mAh/g. After 200 cycles, it remains at 140.1 mAh g<sup>-1</sup>, corresponding to capacity retention of 92.8%. In contrast, the capacity for the cell with 1 M LiPF<sub>6</sub> in EC/PC (7:3, v/v) decays very fast, with only 22.7% retention after 200 cycles. The cell with dual-salt in EC/PC (7:3, v/v) exhibits almost no capacity after 123 cycles. Increasing the content of PC also deteriorates the cycling performance, as the capacity retention of trisalt in EC/PC (5:5, v/v) cell is only 76.6% after 200 cycles. Besides better cycling stability, a higher average CE is also observed in trisalt system (99.7%) than 1 M LiPF<sub>6</sub> (98.6%), dual-salt (98.1%) in EC/PC (7:3, v/v), and trisalt in EC/PC (5:5, v/v) (99.4%) in the first 100 cycles (**Figure S2**). It should be noticed that the anodes are 250 μm thick lithium metals and therefore the capacity ratio of anodes to cathodes is much larger than one.

The cycling stability of trisalt in EC/PC (7:3, v/v) is also reflected by its voltage profile. Its voltage hysteresis only increases slightly from 0.23 V in cycle 1 to 0.32 V in cycle 100 (**Figure 2d**), whereas there are dramatic increases of voltage hysteresis as well as capacity fading for 1 M LiPF<sub>6</sub> (0.17 to 1.10 V, **Figure 2b**) and dual-salt (0.13 to 1.35 V, **Figure 2c**). For trisalt in EC/PC (5:5, v/v), although the voltage hysteresis does not increase remarkably in the first 100 cycles (0.11 to 0.36 V), it increases dramatically afterward (0.36 V in cycle 100 to 0.68 V in cycle 200, **Figure 2e**) compared to trisalt in EC/PC (7:3, v/v) (0.32 to 0.48 V). These larger voltage hysteresis increases may result from faster electrolyte consumption, irreversible Li loss, and more resistive SEI at the lithium anode.<sup>24</sup> Rate performance was further evaluated, which shows that the trisalt in EC/PC (7:3, v/v) electrolyte can work well up to 6 C, of which the specific capacities at 2 C, 4 C, and 6 C are 129.3 mAh g<sup>-1</sup>, 106.5 mAh g<sup>-1</sup>, and 71.6 mAh g<sup>-1</sup>, respectively (**Figure S3**). To further enhance cycling performance, a piece of porous PVdF-HFP film is placed between lithium anode and a conventional separator for the trisalt in EC/PC (7:3, v/v) electrolyte since PVdF-HFP can help better passivate lithium surface and realize more uniform lithium deposition.<sup>30</sup> It also has sufficient thermal stability.<sup>31</sup> With the addition of PVdF-HFP film, the cycling performance is further improved to 97.0% capacity retention after 400 cycles at 0.83 mA cm<sup>-2</sup>, with an average CE of 99.7% (**Figure 2f,g**). All cycling performance shows that trisalt in EC/PC (7:3, v/v) is an applicative electrolyte system for Li/NMC batteries with relatively desirable behavior.

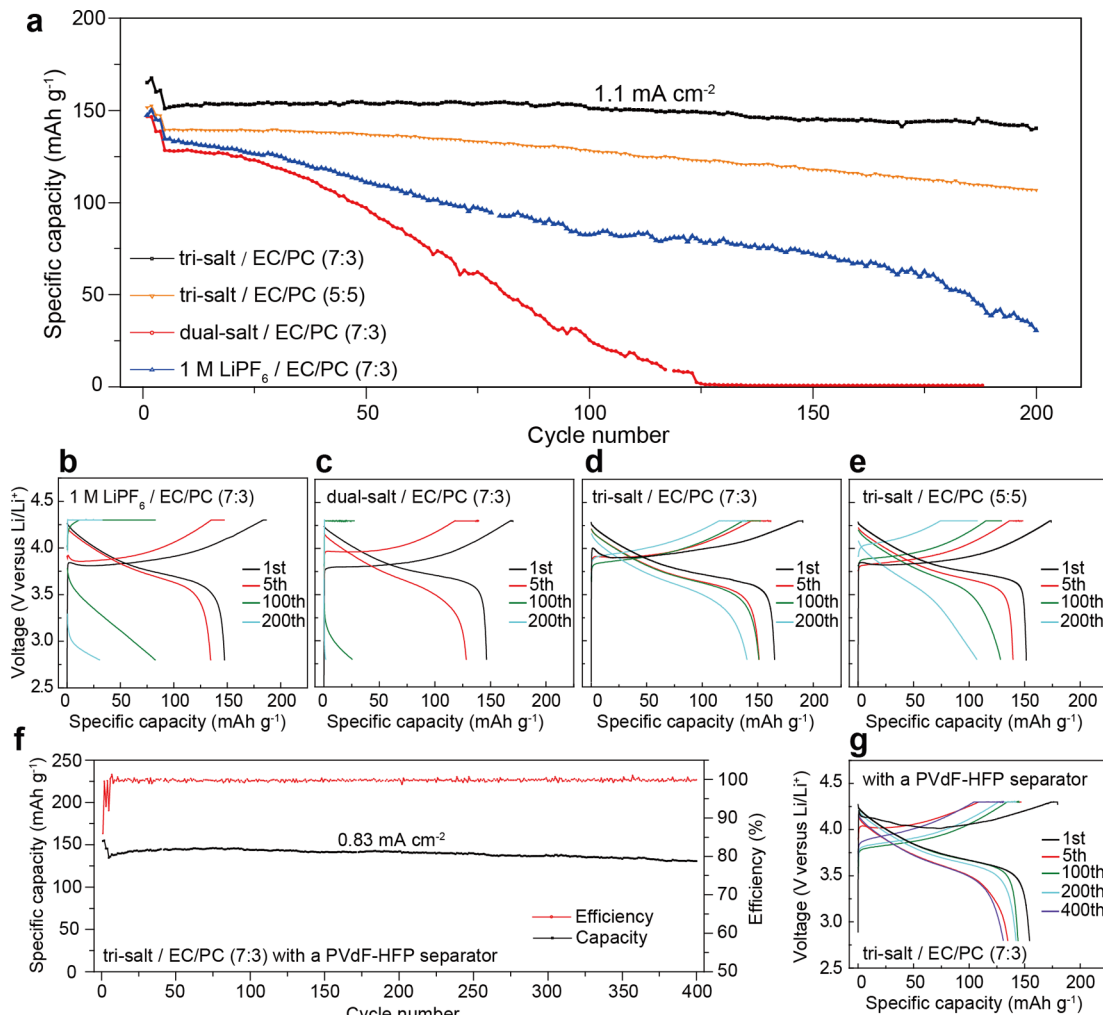


**Figure 2.** Electrochemical behavior of different EC/PC electrolytes for Li/NMC batteries. (a) Cycling performance with different electrolytes at  $1.1 \text{ mA cm}^{-2}$  after 2 cycles at  $0.11 \text{ mA cm}^{-2}$  and two cycles at  $0.37 \text{ mA cm}^{-2}$ . The capacity loadings of all cells are  $1.1 \text{ mAh cm}^{-2}$ . (b–e) Corresponding voltage profiles of Li/NMC batteries in panel a. (b)  $1 \text{ M LiPF}_6$  in EC/PC (7:3), (c) dual-salt in EC/PC (7:3), (d) trisalt in EC/PC (7:3), and (e) trisalt in EC/PC (5:5). (f) Cycling performance with trisalt in EC/PC (7:3) electrolyte and a PVdF-HFP separator. The cell capacity is  $0.83 \text{ mAh cm}^{-2}$  and it was cycled at  $0.83 \text{ mA cm}^{-2}$  after two cycles at  $0.08 \text{ mA cm}^{-2}$  and two cycles at  $0.28 \text{ mA cm}^{-2}$ . (g) Voltage profile of panel f. The first cycles in (b–e,g) are at C/10, while the rest are at 1 C rate. All ratios mentioned are volume ratios.

To elucidate the origin of the difference in electrochemical performance among these electrolyte systems, scanning electron microscope (SEM) and electrochemical impedance spectroscopy (EIS) were used to characterize cells with different electrolytes. First, the morphology of lithium anodes after 100 cycles were examined by SEM.  $1 \text{ M LiPF}_6$  in EC/PC (7:3, v/v) leads to a rigid and brittle SEI at surface, which holistically cracks into pieces due to the large volume change of lithium during cycling (Figure 3a,e), exposing a vast portion of fresh lithium surface to further electrolyte corrosion. The lithium surface with the dual-salt in EC/PC (7:3, v/v) electrolyte shows less cracks, but more uneven bumps and porosity (Figure 3b,f). The cracked regions often appear higher than their surroundings, which can be explained as that lithium grows and breaks the SEI layer, and continuously reacts with the electrolyte. In such dual-salt electrolyte, the cracks mainly happen at localized areas. This suggests that the toughness of SEI is better than  $1 \text{ M LiPF}_6$  in EC/PC so that cracks only happen at scattered weak points without grievous propagation. For the trisalt in EC/PC (7:3, v/v) electrolyte, the SEI layer exhibits a more uniform and smoother surface than the  $1 \text{ M LiPF}_6$  and dual-salt cases (Figure 3c,g). Cracks are observed scarcely. It demonstrates the enhanced uniformity and mechanical strength of the SEI layer. On the other side, increasing PC content to EC:PC = 5:5 (v/v) significantly deteriorates the morphology of SEI. The surface of SEI is full of crevices (Figure 3d,h). This can be explained by that the higher portion of PC attacks lithium, aggravating the corrosion of lithium and exceeding the protective capability of the trisalt system.

The morphology observed in SEM correlates well with EIS results, as better morphology corresponds to less increase in impedance (Figure 3i–l). The cell with trisalt in EC/PC (7:3, v/v) shows a reduced charge transfer resistance ( $R_{ct}$ ) after 100 cycles compared with that after the first two formation cycles, signifying the best SEI quality among the four electrolytes and possibly further amelioration after first two cycles (Figure 3k). Meanwhile,  $R_{ct}$  of  $1 \text{ M LiPF}_6$  in EC/PC (7:3, v/v), dual-salt in EC/PC (7:3, v/v), and trisalt in EC/PC (5:5, v/v) increase by 15%, 82%, and 53%, respectively, due to the poorer SEI. These results reveal that trisalt system indeed improves the behavior of PC-based electrolyte through promoting the

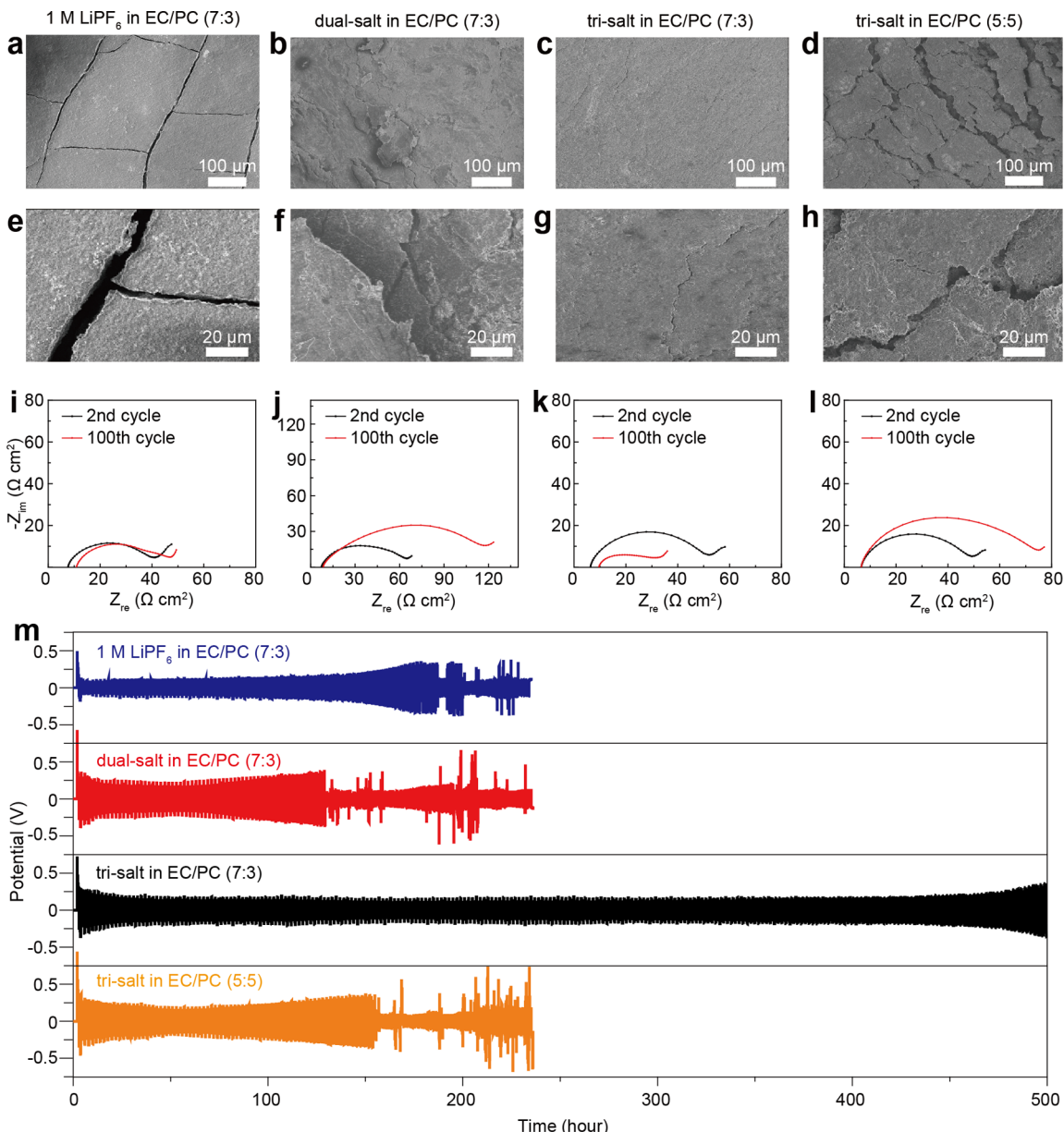


**Figure 3.** Morphology and evolution of Li surfaces. (a–h) Top views of cycled Li anodes retrieved from Li/NMC batteries after 100 cycles with (a,e) 1 M LiPF<sub>6</sub> in EC/PC (7:3), (b,f) dual-salt in EC/PC (7:3), (c,g) trisalt in EC/PC (7:3), and (d,h) trisalt in EC/PC (5:5). (i–l) Nyquist plots of Li/NMC batteries after two cycles and 100 cycles with (i) 1 M LiPF<sub>6</sub> in EC/PC (7:3), (j) dual-salt in EC/PC (7:3), (k) trisalt in EC/PC (7:3), and (l) trisalt in EC/PC (5:5) in the range of 1 MHz to 10 Hz. (m) Cycling performance of Li/Li symmetric batteries of different electrolytes with at a current density of 1 mA cm<sup>-2</sup> and a charge/discharge capacity of 1 mAh cm<sup>-2</sup>. All ratios mentioned are volume ratios.

formation of a high-quality SEI and suppressing the consumption of electrolyte. One thing to notice is that although the trisalt in EC/PC (5:5, v/v) exhibits larger increase in  $R_{\text{ct}}$  than 1 M LiPF<sub>6</sub> in EC/PC (7:3, v/v) after 100 cycles, it has better Li/NMC cycling stability. It is likely that LiBOB can better protect the NMC cathode and Al current collector by forming passivation layer.<sup>24</sup>

The compatibility toward Li metals of these electrolytes was systematically evaluated by carrying out a series of experiments including 250 μm Li/250 μm Li cells (Figure 3m), 250 μm Li/40 μm Li cells (Figure S4), and 250 μm Li/Cu cells (Figure S5). First, in 250 μm Li/250 μm Li cells, the trisalt in EC/PC (7:3, v/v) electrolyte gave the longest cycling performance of over 200 cycles, where the overpotential changes from 206 mV at cycle 5 to 105 and 152 mV at cycle 100 and 200,

respectively. In contrast, 1 M LiPF<sub>6</sub>, dual-salt in EC/PC (7:3, v/v), and trisalt in EC/PC (5:5, v/v) all suffered from failure after tens of cycles, which could be attributed to intermittent collapse of SEI and faster accumulation of the SEI layer. Such trend in the overpotential increase agrees with that of  $R_{\text{ct}}$  in Figure 3i–l.

The next test was based on 250 μm Li/40 μm Li cells with 100 μL electrolyte. The Coulombic efficiency can be estimated when the 40 μm Li (8.25 mAh cm<sup>-2</sup>) is fully consumed (see Figure S4 for detailed calculations). The 1 M LiPF<sub>6</sub>, dual-salt, trisalt in EC/PC (7:3, v/v), and trisalt in EC/PC (5:5, v/v) electrolytes could be charged/discharged for 243, 238, 293, and 154 cycles before ending, which correspond to CE of 93.2%, 93.1%, 94.4%, and 89.3%, respectively. The highest CE

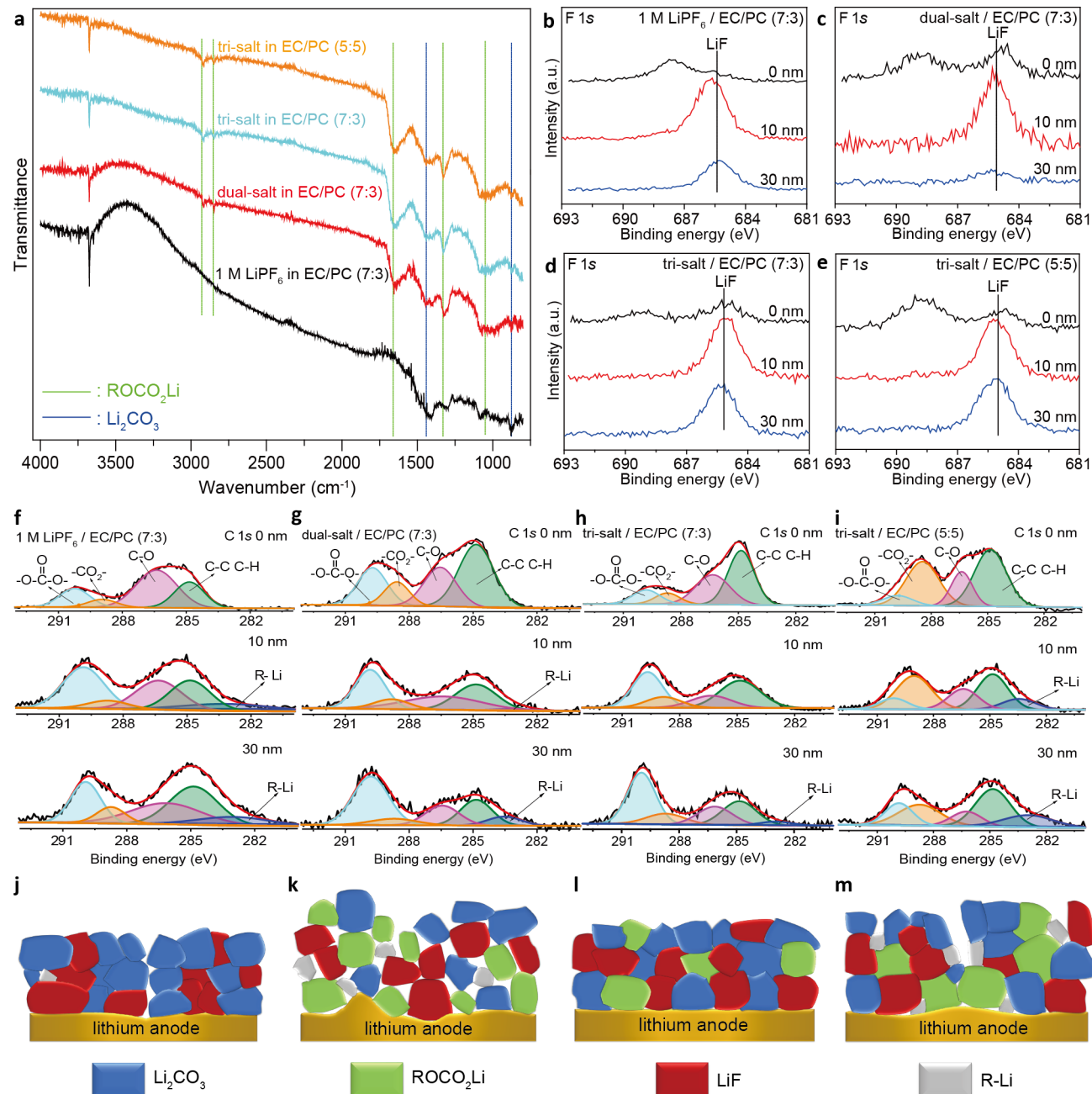


**Figure 4.** FT-IR and XPS characterizations of SEI on Li anodes retrieved from Li/NMC cells after 100 cycles. (a) FT-IR spectra of different electrolytes. (b–e) XPS spectra of F 1s in (b) 1 M LiPF<sub>6</sub> in EC/PC (7:3), (c) dual-salt in EC/PC (7:3), (d) tri-salt in EC/PC (7:3), and (e) tri-salt in EC/PC (5:5). (f–i) XPS spectra of C 1s in (f) 1 M LiPF<sub>6</sub> in EC/PC (7:3), (g) dual-salt in EC/PC (7:3), (h) tri-salt in EC/PC (7:3), and (i) tri-salt in EC/PC (5:5). The 0 nm, 10 nm, and 30 nm indicate the depths at which the spectra were acquired. (j–m) SEI schematics on Li surface with (j) 1 M LiPF<sub>6</sub> in EC/PC (7:3), (k) dual-salt in EC/PC (7:3), (l) tri-salt in EC/PC (7:3), and (m) tri-salt in EC/PC (5:5). All ratios mentioned are volume ratios.

in tri-salt in EC/PC (7:3, v/v) electrolyte indicates that it outperforms other combinations in reducing lithium loss.

Li/Cu cells were also tested to measure CE of lithium deposition (Figure S5). Tri-salt in EC/PC (5:5, v/v) has the lowest CE of 92.9% among these four electrolytes, arising from the intensified attack toward Li due to the higher ratio of PC. In the EC/PC (7:3, v/v) electrolyte system, all 1 M LiPF<sub>6</sub>, dual-salt, and tri-salt electrolytes have similar CE around 94.2%. The results are consistent with the CE calculated based on 250 μm Li/40 μm Li cells (Figure S4).

To further understand mechanisms behind the morphological diversities of these SEI layers, the chemical composition of the SEI layers after 100 cycles were characterized by Fourier-transform infrared (FT-IR) spectroscopy and X-ray photoelectron spectroscopy (XPS) at different depths. Compared to dual-salt and tri-salt systems, a distinct character of 1 M LiPF<sub>6</sub> in EC/PC (7:3, v/v) is the strong signal of Li<sub>2</sub>CO<sub>3</sub> (1520–1450, 875 cm<sup>-1</sup>) and the absence of ROCO<sub>2</sub>Li (3000–2800, 1660, 1320, 1150–1050 cm<sup>-1</sup>) in FT-IR (Figure 4a). In contrast, all other dual-salt and tri-salt systems show stronger ROCO<sub>2</sub>Li peaks than Li<sub>2</sub>CO<sub>3</sub>. In 1 M LiPF<sub>6</sub> in EC/

PC (7:3, v/v), the high portion of inorganic  $\text{Li}_2\text{CO}_3$  in SEI indicates that the corresponding SEI layer is rigid, which leads to the widely distributed cracks observed in Figure 3a. In contrast, the higher portion of  $\text{ROCO}_2\text{Li}$  in dual-salt and trisalt systems means that the SEI is softer than the  $\text{LiPF}_6$ -based electrolyte.

The major difference between the dual-salt and the trisalt electrolytes is that LiF only appears near SEI surface in the dual-salt system, but not deeply inside. In contrast, strong LiF is observed through the whole SEI in trisalt in EC/PC (7:3, v/v). This suggests that the SEI of dual-salt in EC/PC (7:3, v/v) is more heterogeneous, which causes inhomogeneous ion flux and promotes uneven lithium deposition.<sup>21</sup> Therefore, more bumps and porous features are observed in SEM (Figure 3b,f). In contrast, the higher portion of LiF in trisalt system suggests a high-quality SEI to suppress lithium dendrite, consistent with uniform and flat layer shown in Figure 3c and g.

Another difference between trisalt and dual-salt/1 M  $\text{LiPF}_6$  in EC/PC (7:3, v/v) is that the peak area of R-Li ( $\sim 283.5$  eV) at the depth of 30 nm is much smaller in the trisalt system (3.7%), while the values are 11.2% and 8.1% for 1 M  $\text{LiPF}_6$  and dual-salt in EC/PC (7:3, v/v), respectively (Table S1). R-Li is a product of solvent decomposition and detrimental to the strength of SEI due to its low binding energy.<sup>32</sup> Besides salts, the EC/PC ratio also affects the SEI composition. Increasing PC content to EC/PC = 5:5 leads to a higher R-Li content of 16.1% in the SEI and reduces the mechanical strength of SEI (Figure 4i), which likely leads to more porous morphology in SEM (Figure 3d,h).

On the basis of these observations, the improved SEI of trisalt in EC/PC (7:3, v/v) electrolyte may originate from the formation of adequate amount of different components inside. The SEI needs  $\text{Li}_2\text{CO}_3$  to enhance mechanical strength and  $\text{ROCO}_2\text{Li}$  to provide flexibility and bind inorganic components together. EC/PC (7:3, v/v) with a proper salt system can provide a balanced ratio of these two components. The addition of 0.05 M  $\text{LiPF}_6$  into the dual-salt system helps form sufficient amount of LiF without affecting the ratio of  $\text{Li}_2\text{CO}_3/\text{ROCO}_2\text{Li}$ , but too much  $\text{LiPF}_6$  (e.g., 1M) will lead to significant amount of  $\text{Li}_2\text{CO}_3$  but almost no  $\text{ROCO}_2\text{Li}$ , as shown in Figure 4a.

Given these analyses above, by combining merits of electrolyte solvent and salt systems above together, the trisalt in EC/PC (7:3, v/v) helps produce an SEI layer, which contains sufficient amount of both  $\text{Li}_2\text{CO}_3$  to suppress corrosion and  $\text{ROCO}_2\text{Li}$  acting like a binder to hold other SEI components to allow high toughness (Figure 4l). Hence, the SEI quality is in the sequence of trisalt in EC/PC (7:3, v/v)  $>$  1 M  $\text{LiPF}_6$  in EC/PC (7:3, v/v)  $\approx$  trisalt in EC/PC (5:5, v/v)  $>$  dual salt in EC/PC (7:3, v/v), which is consistent with the sequence of impedance increase in EIS and SEM images (Figure 3). These results demonstrate that the trisalt in EC/PC (7:3, v/v) is the optimized one among the four combinations studied as a result of optimized ratio of  $\text{Li}_2\text{CO}_3$ , LiF, and organic species, which leads to high stability in cycling and cell impedance.

### 3. SUMMARY

In summary, we demonstrated a nonflammable electrolyte with EC/PC as the solvent, which can bear the exposure to open butane fire for over 1 min and has reasonable conductivity at low temperatures. The use of LiTFSI/LiBOB/LiPF<sub>6</sub> trisalt is able to effectively restrain the recognized negative effects of PC

on SEI, which allowed 97.0% capacity retention after 400 cycles while cycling with NMC cathodes at moderate current density. SEI layers from this electrolyte are integral and even, as a result of the balance among the amounts of LiF,  $\text{Li}_2\text{CO}_3$  and organic components. Such balance protects lithium from further corrosion and endows favorable strength and toughness to the SEI layer to outlive the volume change of lithium. These results prove that LiTFSI-LiBOB-LiPF<sub>6</sub> in EC/PC electrolyte system is a promising candidate for safe lithium batteries with reasonable liquid temperature window, expecting to promote the development of highly reliable rechargeable lithium metal batteries.<sup>21</sup>

## 4. EXPERIMENTAL SECTION

**4.1. Materials.**  $\text{LiNi}_{1/3}\text{Mn}_{1/3}\text{Co}_{1/3}\text{O}_2$  (NMC) (MSE Supplies LLC), carbon black (Timcal), and PVDF (Arkema Kynar 761) were used for the cathode. LiTFSI (Gotion Inc.), LiBOB (Gotion Inc.), LiPF<sub>6</sub> (Gotion Inc.), EC (99%, Sigma-Aldrich), PC (99.7%, Sigma-Aldrich), and DEC (99%, Sigma-Aldrich) were used to prepare electrolytes in the glovebox with  $\text{H}_2\text{O} < 0.1$  ppm and oxygen  $< 0.1$  ppm. A conventional electrolyte, 1 M  $\text{LiPF}_6$  in EC/DEC (5:5, w/w) (Gotion Inc.) was used for reference. PVDF-HFP (Arkema Kynar 2801) separators were prepared by a phase-inversion process as described in the Supporting Information. Except for PVDF, which was dried at 70 °C for 24 h before use, all other materials were used as received.

**4.2. Battery Assembly and Electrochemical Measurements.**

NMC cathodes preparation process was described in the Supporting Information. Lithium metal batteries were assembled with the NMC cathode, 250  $\mu\text{m}$  thick lithium metal anode, two pieces of Celgard 3501 separators, and as-prepared electrolytes (120  $\mu\text{L}$  in each cell) in CR2032 coin cells. Li/Li batteries were assembled with the 250 or 40  $\mu\text{m}$  thick lithium metals, two pieces of Celgard 3501 separators and as-prepared electrolytes (100  $\mu\text{L}$  in each cell) in CR2032 coin cells. Li/Cu batteries were assembled with the 250  $\mu\text{m}$  thick lithium metals and Cu foil, two pieces of Celgard 3501 separators, and as-prepared electrolytes (100  $\mu\text{L}$  in each cell) in CR2032 coin cells. All the EIS tests were conducted by Biologic VMP3 multichannel potentiostat from Bio-Logic in a frequency range of 1 MHz to 10 Hz with a 20 mV amplitude. The galvanostatic cycling was performed between 2.8 and 4.3 V by Landt battery testers.

**4.3. Thermal Tests and Material Characterization.** The DSC measurements were performed by Discovery DSC250 in the temperature range from 40 °C to -70 °C at a 5 °C  $\text{min}^{-1}$  cooling rate. Solidification and ignition tests were described in the Supporting Information. Lithium anodes for characterizations were harvested from disassembled cycled cells and rinsed by PC to remove the electrolyte residue before drying under vacuum. The morphologies of lithium anodes were characterized on SIGMA VP Zeiss SEM at 3.0 kV. Surface analysis of the anodes at different depths was performed by a PHI 5500 XPS with a monochromatic Al K $\alpha$  X-ray excitation source (1486.6 eV) and a Spectrum 400 FT-IR spectrometer. All the sample transfer processes were protected by argon gas.

## ■ ASSOCIATED CONTENT

**S Supporting Information**

The Supporting Information is available free of charge on the ACS Publications website at DOI: 10.1021/acsami.8b22156.

Additional physical, electrochemical, and XPS test data (PDF)

Video of flammability test of trisalt in EC-PC electrolyte (AVI)

Video of flammability test of LiPF<sub>6</sub> and trisalt in EC-DEC electrolyte (AVI)

Video of flammability test of LiPF<sub>6</sub> and dual-salt in EC-PC electrolyte (AVI)

## AUTHOR INFORMATION

### Corresponding Author

\*E-mail: [yy2664@columbia.edu](mailto:yy2664@columbia.edu).

### ORCID

Tianwei Jin: [0000-0002-4355-5474](https://orcid.org/0000-0002-4355-5474)

Xue Wang: [0000-0003-3257-0668](https://orcid.org/0000-0003-3257-0668)

Haowei Zhai: [0000-0002-7030-3563](https://orcid.org/0000-0002-7030-3563)

Yuan Yang: [0000-0003-0264-2640](https://orcid.org/0000-0003-0264-2640)

### Notes

The authors declare no competing financial interest.

## ACKNOWLEDGMENTS

The authors greatly appreciate the funding support from AFOSR (FA9550-18-1-0410).

## REFERENCES

- (1) Tarascon, J. M.; Armand, M. Issues and challenges facing rechargeable lithium batteries. *Nature* **2001**, *414* (6861), 359–367.
- (2) Kim, H.; Jeong, G.; Kim, Y.-U.; Kim, J.-H.; Park, C.-M.; Sohn, H.-J. Metallic anodes for next generation secondary batteries. *Chem. Soc. Rev.* **2013**, *42* (23), 9011–9034.
- (3) Kang, K.; Meng, Y. S.; Bréger, J.; Grey, C. P.; Ceder, G. Electrodes with High Power and High Capacity for Rechargeable Lithium Batteries. *Science* **2006**, *311* (5763), 977–980.
- (4) Li, H.; Wang, Z.; Chen, L.; Huang, X. Research on Advanced Materials for Li-ion Batteries. *Adv. Mater.* **2009**, *21* (45), 4593–4607.
- (5) Suo, L.; Borodin, O.; Gao, T.; Olguin, M.; Ho, J.; Fan, X.; Luo, C.; Wang, C.; Xu, K. Water-in-salt” electrolyte enables high-voltage aqueous lithium-ion chemistries. *Science* **2015**, *350* (6263), 938–943.
- (6) Choi, N.-S.; Chen, Z.; Freunberger, S. A.; Ji, X.; Sun, Y.-K.; Amine, K.; Yushin, G.; Nazar, L. F.; Cho, J.; Bruce, P. G. Challenges Facing Lithium Batteries and Electrical Double-Layer Capacitors. *Angew. Chem., Int. Ed.* **2012**, *51* (40), 9994–10024.
- (7) Sun, Y.-K.; Myung, S.-T.; Park, B.-C.; Prakash, J.; Belharouak, I.; Amine, K. High-energy cathode material for long-life and safe lithium batteries. *Nat. Mater.* **2009**, *8*, 320–324.
- (8) Li, N.-W.; Yin, Y.-X.; Yang, C.-P.; Guo, Y.-G. An Artificial Solid Electrolyte Interphase Layer for Stable Lithium Metal Anodes. *Adv. Mater.* **2016**, *28* (9), 1853–1858.
- (9) Arai, J. A novel non-flammable electrolyte containing methyl nonafluorobutyl ether for lithium secondary batteries. *J. Appl. Electrochem.* **2002**, *32* (10), 1071–1079.
- (10) Xu, K. Nonaqueous Liquid Electrolytes for Lithium-Based Rechargeable Batteries. *Chem. Rev.* **2004**, *104* (10), 4303–4418.
- (11) Smagin, A. A.; Matyukha, V. A.; Korobtsev, V. P. Application of thermogravimetric studies for optimization of lithium hexafluorophosphate production. *J. Power Sources* **1997**, *68* (2), 326–327.
- (12) Chou, S.-L.; Wang, J.-Z.; Sun, J.-Z.; Wexler, D.; Forsyth, M.; Liu, H.-K.; MacFarlane, D. R.; Dou, S.-X. High Capacity, Safety, and Enhanced Cyclability of Lithium Metal Battery Using a V2O5 Nanomaterial Cathode and Room Temperature Ionic Liquid Electrolyte. *Chem. Mater.* **2008**, *20* (22), 7044–7051.
- (13) Farnicola, A.; Croce, F.; Scrosati, B.; Watanabe, T.; Ohno, H. LiTFSI-BEPyTFSI as an improved ionic liquid electrolyte for rechargeable lithium batteries. *J. Power Sources* **2007**, *174* (1), 342–348.
- (14) Wu, L.; Song, Z.; Liu, L.; Guo, X.; Kong, L.; Zhan, H.; Zhou, Y.; Li, Z. A new phosphate-based nonflammable electrolyte solvent for Li-ion batteries. *J. Power Sources* **2009**, *188* (2), 570–573.
- (15) Ota, H.; Kominato, A.; Chun, W.-J.; Yasukawa, E.; Kasuya, S. Effect of cyclic phosphate additive in non-flammable electrolyte. *J. Power Sources* **2003**, *119*–*121*, 393–398.
- (16) Suo, L.; Hu, Y.-S.; Li, H.; Armand, M.; Chen, L. A new class of Solvent-in-Salt electrolyte for high-energy rechargeable metallic lithium batteries. *Nat. Commun.* **2013**, *4*, 1481.
- (17) Zeng, Z.; Murugesan, V.; Han, K. S.; Jiang, X.; Cao, Y.; Xiao, L.; Ai, X.; Yang, H.; Zhang, J.-G.; Sushko, M. L.; Liu, J. Non-flammable electrolytes with high salt-to-solvent ratios for Li-ion and Li-metal batteries. *Nature Energy* **2018**, *3* (8), 674–681.
- (18) Fan, X.; Chen, L.; Borodin, O.; Ji, X.; Chen, J.; Hou, S.; Deng, T.; Zheng, J.; Yang, C.; Liou, S.-C.; Amine, K.; Xu, K.; Wang, C. Non-flammable electrolyte enables Li-metal batteries with aggressive cathode chemistries. *Nat. Nanotechnol.* **2018**, *13* (8), 715–722.
- (19) Chen, S.; Zheng, J.; Yu, L.; Ren, X.; Engelhard, M. H.; Niu, C.; Lee, H.; Xu, W.; Xiao, J.; Liu, J.; Zhang, J.-G. High-Efficiency Lithium Metal Batteries with Fire-Retardant Electrolytes. *Joule* **2018**, *2* (8), 1548–1558.
- (20) Aurbach, D.; Daroux, M. L.; Faguy, P. W.; Yeager, E. Identification of Surface Films Formed on Lithium in Propylene Carbonate Solutions. *J. Electrochem. Soc.* **1987**, *134* (7), 1611–1620.
- (21) Aurbach, D.; Gofer, Y.; Langzam, J. The Correlation Between Surface Chemistry, Surface Morphology, and Cycling Efficiency of Lithium Electrodes in a Few Polar Aprotic Systems. *J. Electrochem. Soc.* **1989**, *136* (11), 3198–3205.
- (22) Ding, M. S.; Xu, K.; Zhang, S.; Jow, T. R. Liquid/Solid Phase Diagrams of Binary Carbonates for Lithium Batteries Part II. *J. Electrochem. Soc.* **2001**, *148* (4), A299–A304.
- (23) Zheng, J.; Engelhard, M. H.; Mei, D.; Jiao, S.; Polzin, B. J.; Zhang, J.-G.; Xu, W. Electrolyte additive enabled fast charging and stable cycling lithium metal batteries. *Nature Energy* **2017**, *2*, 17012.
- (24) Chen, X.; Xu, W.; Engelhard, M. H.; Zheng, J.; Zhang, Y.; Ding, F.; Qian, J.; Zhang, J.-G. Mixed salts of LiTFSI and LiBOB for stable LiFePO4-based batteries at elevated temperatures. *J. Mater. Chem. A* **2014**, *2* (7), 2346–2352.
- (25) Lu, Z.; Yang, L.; Guo, Y. Thermal behavior and decomposition kinetics of six electrolyte salts by thermal analysis. *J. Power Sources* **2006**, *156* (2), 555–559.
- (26) Xu, K.; Zhang, S.; Jow, T. R.; Xu, W.; Angell, C. A. LiBOB as Salt for Lithium-Ion Batteries: A Possible Solution for High Temperature Operation. *Electrochim. Solid-State Lett.* **2002**, *5* (1), A26–A29.
- (27) McEwen, A. B.; Ngo, H. L.; LeCompte, K.; Goldman, J. L. Electrochemical Properties of Imidazolium Salt Electrolytes for Electrochemical Capacitor Applications. *J. Electrochem. Soc.* **1999**, *146* (5), 1687–1695.
- (28) Zhang, X.-x.; Fan, Y.-f.; Tao, X.-m.; Yick, K.-l. Crystallization and prevention of supercooling of microencapsulated n-alkanes. *J. Colloid Interface Sci.* **2005**, *281* (2), 299–306.
- (29) Ding, M. S.; Xu, K.; Jow, T. R. Liquid/Solid Phase Diagrams of Binary Carbonates for Lithium Batteries. *J. Electrochem. Soc.* **2000**, *147* (5), 1688–1694.
- (30) Luo, J.; Fang, C.-C.; Wu, N.-L. High Polarity Poly(vinylidene difluoride) Thin Coating for Dendrite-Free and High-Performance Lithium Metal Anodes. *Advanced Energy Materials* **2018**, *8* (2), 1701482.
- (31) Du Pasquier, A.; Warren, P. C.; Culver, D.; Gozdz, A. S.; Amatucci, G. G.; Tarascon, J. M. Plastic PVDF-HFP electrolyte laminates prepared by a phase-inversion process. *Solid State Ionics* **2000**, *135* (1), 249–257.
- (32) Ota, H.; Sakata, Y.; Inoue, A.; Yamaguchi, S. Analysis of Vinylene Carbonate Derived SEI Layers on Graphite Anode. *J. Electrochem. Soc.* **2004**, *151* (10), A1659–A1669.